Improved tribological performance of a-C:H/a-C:H:Si:O coated polyether ether ketone by introducing graded interfacial structure

Xianchun Jiang [b], Lingkang Meng [b], Peng Guo [a,**], Rende Chen [a], Zhenyu Wang [a], Hao Li [a], Kazuhito Nishimura [a], Aiying Wang [a,c], Peiling Ke [a,c,*] (ID)

[a] State Key Laboratory of Advanced Marine Materials, Zhejiang Key Laboratory of Extreme-environmental Material Surfaces and Interfaces, Ningbo Institute of Materials Technology and Engineering, Chinese Academy of Sciences, Ningbo, 315201, China
[b] The State Key Laboratory of Digital Manufacturing Equipment and Technology, School of Mechanical Science and Engineering, Huazhong University of Science and Technology, Wuhan, 430074, China
[c] Center of Materials Science and Optoelectronics Engineering, University of Chinese Academy of Sciences, Beijing, 100049, China

ARTICLE INFO

ABSTRACT

Carbon-based coatings have been successfully utilized in aerospace, automobiles, and ocean exploration, as typical solid lubricants. Particularly, amorphous carbon coatings (a-C:H) have been employed on kinematic pairs of advanced equipment, such as polyether ether ketone (PEEK)/steel pair, for enhancing their wear resistance and solid lubricity. However, the significant disparity in mechanical properties between PEEK and a-C:H and the poor interface adhesion strength are the key factors that limit the further improvement of tribological performance. In this study, based on the gradient transition of composition and mechanical properties between PEEK and a-C:H, a-C:H/a-C:H:Si:O functionally graded coatings (FGCs) were fabricated on PEEK. The friction behavior of the a-C:H/a-C:H:Si:O FGCs coated PEEK sliding against 304 stainless steel was performed in dry atmosphere using a ball-on-plate reciprocating tribometer. Compared with the single-layer a-C:H and a-C:H:Si:O coated PEEK, the friction stability period of FGCs is extended by at least 33 %. When the thickness ratio of a-C:H/a-C:H:Si:O is 1/1, the wear rate of FGC is as low as 5.6×10^{-7} mm^3/Nm. The excellent tribological performances of FGCs can be attributed to the appropriate mechanical property transition and strong adhesion strength between the coatings and the PEEK. The finite element simulation results indicate that the FGCs can provide more excellent deformation resistance and can also significantly eliminate stress concentration. This work can provide basic theoretical guidance for preparing functionally graded amorphous carbon coatings on PEEK to achieve excellent tribological and wear performance.

1. Introduction

Owing to the lightweight, chemical inertness, and superior mechanical characteristics [1–3], polyether ether ketone (PEEK) and its composites have found extensive application in various industrial fields, including aerospace, biomedical engineering, and ocean exploration [4–8]. Moreover, given its outstanding self-lubricating performance, PEEK emerges as a promising candidate for friction parts or solid lubricant when paired with metals, especially where dry sliding or insufficient lubrication is required [9–12].

However, during the operation of dry or insufficient lubrication

system, PEEK exhibits high friction coefficient and high wear rate against friction pairs such as stainless steel [11,13] and ceramics [14]. This is crucial for the safe and reliable operation of some advanced equipment. To date, two main strategies have been adopted to enhance its wear resistance. For one thing, a number of fillers can be added to PEEK, including carbon fiber (CF), silicon carbide (SiC), zirconium oxide (ZrO$_2$), and graphene oxide (GO), to enhance its mechanical strength and wear resistance [15,16]. Considering that the wear mainly occurs on the surface of PEEK, a protective coating can provide another effective solution, such as Cr$_2$AlC coating [17], Al$_2$O$_3$/PTFE composite coating [18], and NiB-Al$_2$O$_3$ coating [19]. In some practical applications, there
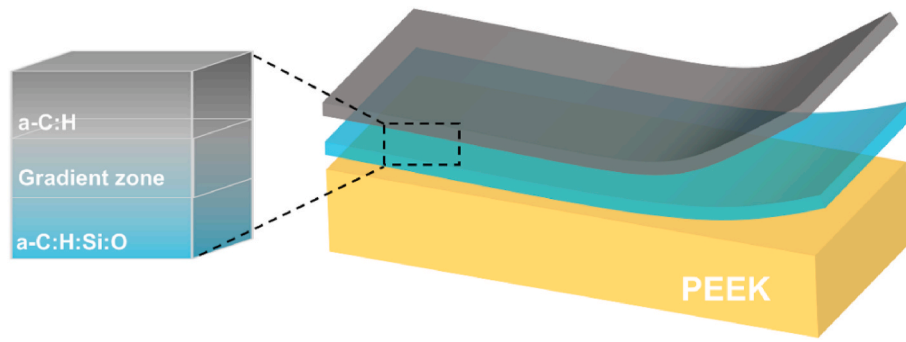
Fig. 1. Structure diagram of the a-C:H/a-C:H:Si:O FGCs.

is a simultaneous requirement for a low wear rate and low friction of the PEEK/metal pair in the motion systems. Amorphous carbon coatings (a-C:H or DLC), which possess excellent anti-wear and anti-friction properties, are considered as one of the most promising materials to address the mentioned issue [20–22].

Up to now, the easy peel-off of the hard a-C:H from the soft PEEK is unfavourable to the high reliability of many applications. Since the high internal stress of a-C:H, which is around 6 GPa, and the poor adhesion strength between a-C:H and PEEK can easily lead to many cracks during the friction test [21,23]. Introducing dopants or alloying elements into a-C:H offers the possibility to modify both the internal stress and interfacial characteristic. Recent studies have confirmed that silicon and oxygen co-doped a-C:H coating (a-C:H:Si:O) through organic precursor of hexamethyl disiloxane (HMDSO) has lower internal stress and a similar composition to PEEK [24–26]. Specifically, low concentrations of Si and O, ranging from 3.96 to 7.49 at.% and from 3.07 to 6.07 at.%, can endow a-C:H:Si:O coatings with excellent adhesion strength, mechanical properties, and wear resistance [27].

From the perspective of interface technology, functionally graded coatings (FGCs) developed from multilayer coatings have provided a new solution to improve protective performance of the coated PEEK. With functionally graded transition achieved through gradient changes in microstructure porosity or composition in the FGCs [28–30], the crack sensitivity can be greatly reduced by eliminating the sharp transition between substrates and coatings [31–33]. For practical applications, the thickness, components and microstructure of functionally graded layer can affect the tribological performance. Besides, different from FGCs on some rigid substrates, the FGCs coated PEEK will exhibit various stress distribution and deformation characteristics under applied normal load, which can result in different tribological behaviors. How to obtain optimum gradient design for FGCs on PEEK and to reveal the role of interface characteristics on the tribological failure mechanism remain unclear.

In the present work, a-C:H/a-C:H:Si:O FGCs with varying compositions and mechanical property gradients were prepared on PEEK by adjusting the thickness ratio of the a-C:H and a-C:H:Si:O coatings. The influence of the composition and microstructure characteristics of the graded interfacial structure on the adhesion strength and mechanical properties of the coatings is investigated. Additionally, the role of interface characteristics and the related friction and wear mechanism of the coated PEEK are also discussed using the finite element method (FEM) model.

Table 2
Deposition parameters of the coatings.

Sample	S1	S2	S3	S4	S5
a-C:H/a-C:H:Si:O	a-C:H	9/1	1/1	1/9	a-C:H:Si:O
Thickness (μm)	1.45 ± 0.05				

2. Experimental details

2.1. Preparation of FGCs

In this work, the substrates employed are P-type silicon wafer and PEEK (20 mm × 20 mm × 20 mm). The hardness (H) and elastic modulus (E) of PEEK are 0.2 GPa and 4.4 GPa, respectively. The a-C:H/a-C:H:Si:O FGCs were prepared by the plasma-enhanced chemical vapor deposition (PECVD) system using the mixture of acetylene (C_2H_2) and HMDSO. The details of cleaning and etching treatment prior to coatings deposition have been described in previous literature [27].

To obtain optimum gradient design, a-C:H/a-C:H:Si:O FGCs with varying compositions and mechanical property gradients were prepared. As depicted in Fig. 1, the functionally graded amorphous carbon coating consist of one bottom-layer of a-C:H:Si:O and a top-layer of a-C:H. The a-C:H:Si:O coating was prepared with a precursor gas HMDSO/C_2H_2 ratio of 1/6, based on our previous study. Additionally, single-layer a-C:H coating (S1) and single-layer a-C:H:Si:O coating (S5) were also prepared as references. The specific deposition parameters are presented in Table 1. It should be noted that when the bottom a-C:H:Si:O coating is deposited, the HMDSO valve is immediately closed, and the flow rate of C_2H_2 is adjusted to 100 sccm for the deposition of a-C:H. Thus, the residual HMDSO can prevent the sharp transition between a-C:H and a-C:H:Si:O. The samples are named S1-S5 according to the thickness ratio of a-C:H to a-C:H:Si:O, as shown in Table 2. All the coatings are maintained at 1.45 ± 0.05 μm by adjusting the deposition time, which is verified by a surface profilometer (Alpha-step IQ, USA).

2.2. Characterization method

The distribution of C, Si and O elements from the coating surface to the substrate was carried out using glow discharge optical emission spectroscopy (GD-OES, Spectrum Analytik GmbH GDA 750HP). Additionally, the depth profile of the chemical composition was obtained by X-ray photoelectron spectroscopy (XPS, Axis UltraDLD, Japan). Moreover, XPS spectra were collected in detail for C 1s, O 1s, and Si 2p peaks.

Table 1
Detailed process parameters of prepared a-C:H/a-C:H:Si:O coatings.

Process	Negative Pulse Voltage (V)	Current (A)	Chamber Pressure (mTorr)	Ar (sccm)	HMDSO (sccm)	C_2H_2 (sccm)	Deposition Rate (nm/min)
Etching	500	0.4	20	100	/	/	/
a-C:H	450	0.3	15	/	/	100	13.5
a-C:H:Si:O					10	60	16.0

The binding energy was calibrated with the C 1s peak at 284.6 eV. A Raman spectrometer (Renishaw, in Via Reflex, 532 nm) was used to analyze the chemical composition related to the bond structure of a-C: H/a-C:H:Si:O coatings, wear tracks and wear scars after the tribological test. In addition, the Raman signal of PEEK was also analyzed at an excitation wavelength of 785 nm [34].

To acquire the mechanical properties of the coatings, their hardness (H) and elastic modulus (E) were measured by a nanoindenter (Nano-Indentation G200, MTS, USA) equipped with a Berkovich-diamond indenter. The values of H and E were calculated using the model proposed by Oliver and Pharr [35,36]. For each sample, at least six different positions were tested, and the average value was calculated to reduce the measurement errors. The residual stress (RS) was calculated in accordance with the Stoney equation [37]. The film/substrate curvature was determined by a laser tester (JLCST022, J&L Tech). The adhesion strength was determined as the maximum tensile strength applied by a direct load perpendicular to the surface under teste. The pull-off test was classified as a near-to-surface, partially destructive method that can measure tensile strength between the coating and the substrate [38,39]. Here, a cylindrical pin with a diameter of 10 mm was adhered to the coated PEEK by epoxy resin AB glue (DP460). The tests were performed using displacement control at 1 mm/min until the coating was completely detached from the substrate. At this point, the adhesion stress was defined as the ratio between the failure load and the test area.

2.3. Tribological tests

The tribological behavior of the coated PEEK was investigated using a ball-on-plate reciprocating tribometer (UMT-3) in ambient air. Owing to its favorable comprehensive properties and low cost, 304 stainless steel is widely utilized in industrial fields, and its frictional characteristics with PEEK have also drawn extensive attention [11,40–42]. Therefore, in this work, the 304 stainless steel (304 L) ball with a diameter of 6 mm serves as the counterpart. The amplitude and sliding velocity were set at 5 mm and 0.05 m · s^{-1} respectively. The normal applied load was 3 N, and the total sliding distance was 180, 75, and 9 m respectively. The PV (product of contact pressure and sliding speed) value corresponding to the test condition ranged from 13.2 to 16.2 MPa m/s. The test condition was chosen to simulate extreme conditions in engineering applications, such as the piston-cylinder friction pair in a piston pump. In addition, this test condition is consistent with the previous studies [27,43]. Each sample was repeated three times under the same sliding conditions to ensure the authenticity and repeatability of the test data. Finally, the wear rate (W, mm^3/N·m) can be calculated by the following equation [44]:

$$W = \frac{V}{FL}$$

where V indicates the wear volume loss (mm^3), F denotes the applied load (N), and L is the total sliding distance (m). The V of coatings is the average value calculated at different locations on the wear track. Following the tribotest, the wear volume of the coated PEEK is obtained by a white light interferometer microscope (UP-Lambda). The surface morphology and chemical composition of the coatings and mating balls were investigated using a scanning electron microscope (SEM, FEI Quanta FEG 250) equipped with an energy dispersive spectrometer (EDS). The transfer film or tribo-film on the surface of the mating balls at different friction stages is observed using an optical microscope (LSM700).

2.4. Finite element method model

The finite element software (ANSYS 2024) was employed to simulate the stress distribution and deformation of different systems. A two-dimensional FEM was developed to simulate the situation when loads

Table 3
Materials properties used in finite element analyses.

Material	Young's modulus, E (GPa)	Poisson's ratio	Density (g/cm^3)	Reference
PEEK	4.4	0.3	1.3	[45,46]
304 L	215.3	0.29	7.9	[47,48]
a-C:H	53.9	0.07	2.5	[49–51]
a-C:H:Si: O	36.7	0.07	2.5	
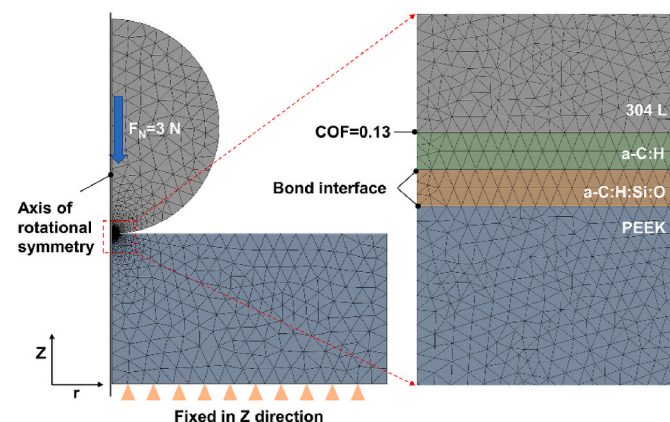
Fig. 2. Schematic of the model and mesh generation of the finite element analysis.

were applied to the system. The physical properties parameters of materials are presented in Table 3. In the model design, a double-layer coating with a thickness ratio of 1:1 was utilized to replace the FGC, as shown in Fig. 2. The total thickness of the coating in all models was 1.5 μm. Furthermore, to avoid any artificial constraints or edge effects, a large substrate region with a diameter of 10 mm and a height of 3 mm was modeled. The diameter of the 304 L ball is 6 mm. Mapped meshing with significant refinement around the contact region results in approximately 406248 triangular elements, with a minimum element size of 7.5×10^{-4} mm. The applied boundary conditions are shown in Fig. 2.

3. Results

3.1. Composition and microstructure characteristics

Fig. 3 shows GD-OES in-depth profiles from five different coatings on the Si wafer. The gradients of C, Si, and O elements have a certain correlation with the thickness ratio of a-C:H and a-C:H:Si:O coatings. For single-layer samples in Fig. 3(a–e), elemental transition is only observed at the coating-substrate interface, with sharp step changes in elemental signals. For FGCs with a-C:H/a-C:H:Si:O thickness ratio of 9/1 (S2), its depth profiles of elements are similar to S1, as observed in Fig. 3(b). However, when the thickness ratio is 1/1 (S3), two curve inflection points appear. At this point, the typical silicon content first remains at 3.3 at.%, then slowly increases to 8.5 at.%, and rises again at the coating-substrate interface(Fig. 3(c)). Similarly, at thickness ratio of 1/9 (S4), the Si content rapidly increases from 3.3 at.% to 8.5 at.% at a depth of 0.15 μm, and this Si content remains stable until the detection depth reaches the coating-substrate interface(Fig. 3(d)).

As shown in Fig. 4, before etching treatment, the O content on the surface is the highest, approximately 8.3 at.%, mainly attributed to the adsorption of O in the air. As the XPS etching time extends, the O content drops sharply within the first 6 min and remains at around 0.6 at.% in the following 42 min. From the etching time of 42 min–72 min, both the O and Si contents increase slowly from 0.6 at.% and 0.1 at.% to 4.0 at.%
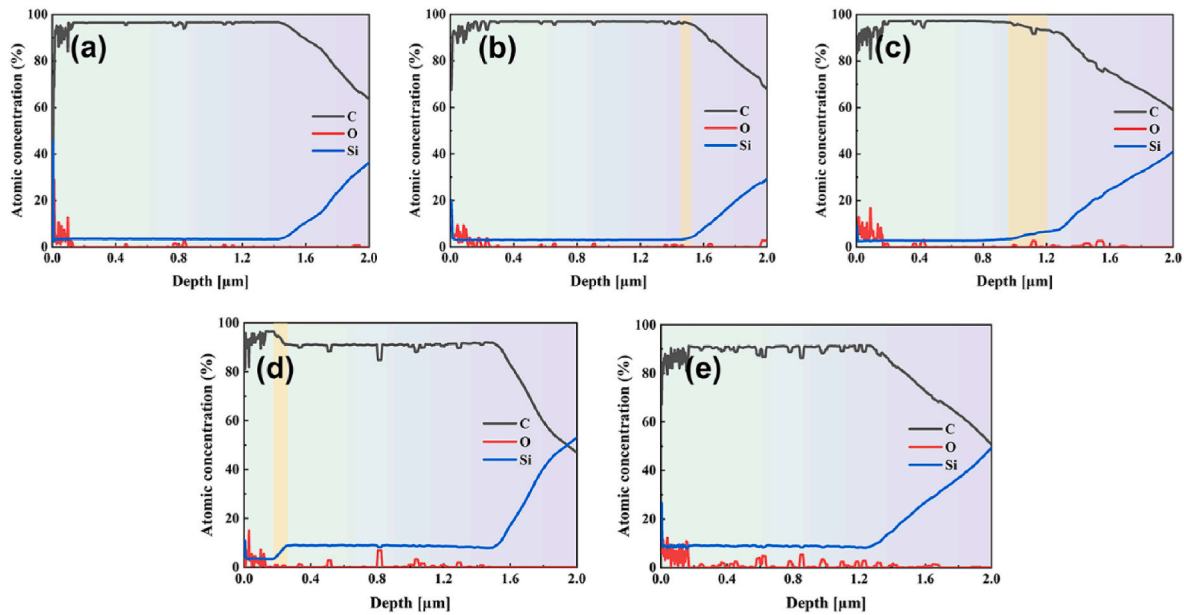
Fig. 3. GD-OES depth profiles of coatings: (a) ~ (e) corresponding S1 ~ S5 samples.
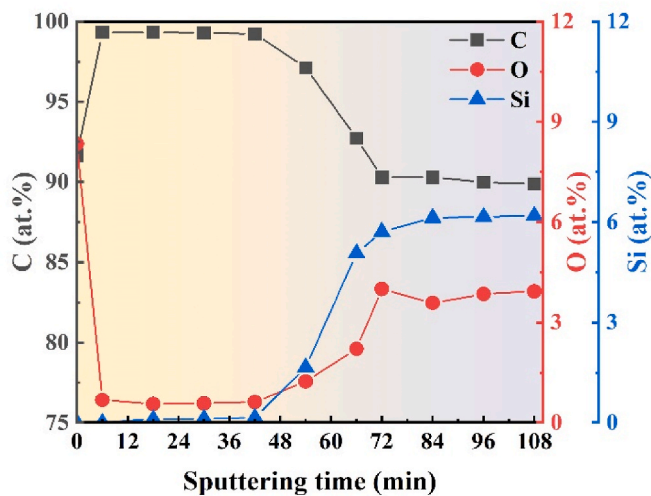

Fig. 4. XPS in-depth profile of the a-C:H/a-C:H:Si:O FGC (Results from S4).

Table 4
Fitting results of C1s peaks at different etching times.

Sputtering time(min)	6	54	66	96
sp^2-C/C-Si-O(%)	52.2	60.3	75.6	78.3
sp^3-C(%)	40.3	33.4	16.2	15.7
C-O(%)	7.5	6.3	8.1	6.0

and 5.7 at.%, respectively. Regarding the C element, its content decreases from 91.7 at.% to 89.9 at.% as the etching time increases. According to the C 1s fitting results at 6, 54, 66, and 96 min, the sp^2-C/C-Si-O content gradually increases, while the sp^3-C content shows an opposite trend, as presented in Table 4. In this work, FGCs are successfully prepared on PEEK, and the significant changes in composition from PEEK to the a-C:H layer are avoided.

The Raman spectra and fitting results of as-deposited FGCs are shown in Fig. 5. In Fig. 5(a), all coatings exhibit typical Raman characteristics of amorphous carbon. Since the top layer of the a-C:H/a-C:H:Si:O FGCs is a-C:H, S1 to S3 have similar G-peak positions and the same half-peak

full width of G-peak (FWHM). The G-peak positions of S1, S2, and S3 are 1537, 1534 and 1536 cm^{-1}, respectively, and the FWHM(G) is 191 cm^{-1}(Fig. 5(b)). The G-peak positions of S4 and S5 is 1531 cm^{-1} and 1520 cm^{-1} respectively, and FWHM(G) are 189 cm^{-1} and 181 cm^{-1} respectively. Thus, the a-C:H:Si:O coating has a lower sp^2-C content and a more ordered structure than the a-C:H coating. The I_D/I_G of all coatings remains around 0.6, indicating that Si and O co-doping has no significant effect on the size of sp^2-C clusters. Compared with other samples, the G-peak position and FWHM(G) of S5 are the smallest, indicating its lowest content of sp^2-C and highest degree of order.

3.2. Mechanical properties

Fig. 6 shows the H, E, H/E, and H3/E2 of the coatings deposited on silicon wafer. Fig. 6(a) demonstrates that the single-layer a-C:H coating achieves the highest hardness of 26.4 GPa and elastic modulus of 215.2 GPa, while the single-layer a-C:H:Si:O coating exhibits the lowest values, at 16.0 GPa and 135.7 GPa, respectively. The FGCs display intermediate mechanical properties, and its mechanical properties exhibit a discernible degradation trend as the thickness of the a-C:H:Si:O layer increases. Generally, the hardness-to-modulus ratio (H/E) quantifies resistance to elastic deformation, and the H^3/E^2 ratio measures resistance to plastic deformation [52]. So, the gradient structural designs enhance resistance to elastic deformation, as evidenced by consistently higher H/E values in gradient coatings, as shown in Fig. 6(b). More specifically, the H/E value of S4 is 13 % greater than that of the single-layer a-C:H:Si:O coating (S5). With regard to plastic deformation, the H^3/E^2 value remains at 0.40 GPa for samples with a-C:H:Si:O layer thickness proportions of 0–50 % (S1–S3) and decreases slightly to 0.36 GPa in S4, which still exceeds the 0.22 GPa for the single-layer a-C:H:Si:O coating (S5). It can be readily concluded that, gradient structural design substantially enhances the comprehensive mechanical properties of amorphous carbon coatings.

As shown in Fig. 7, the single-layer a-C:H exhibits the highest compressive RS (−2.61 GPa), while the single-layer a-C:H:Si:O shows the lowest value (−1.16 GPa). As the thickness ratio increases, the absolute value of compressive RS decreases, demonstrating that the functional gradient design effectively reduces the compressive RS of a-C:H.

Table 5 summarizes the maximum pull-off forces, stress, and fracture types of the pull-off testing of the five samples. In Fig. S1, we provide a schematic diagram of the pull-off test and show the raw data using S5 as an example. The single-layer a-C:H:Si:O coating has the highest
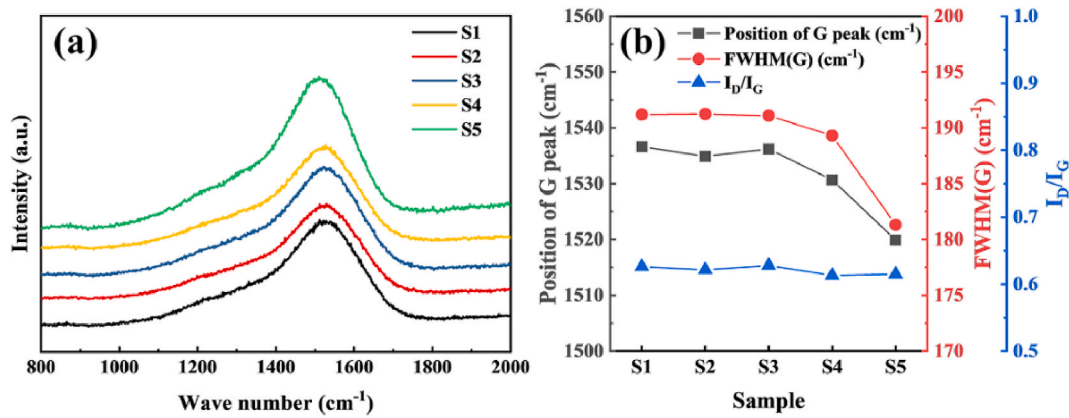
Fig. 5. (a)Raman spectra of as-deposited coatings and (b)the corresponding fitted result of I_D/I_G, position(G), and FWHM(G).
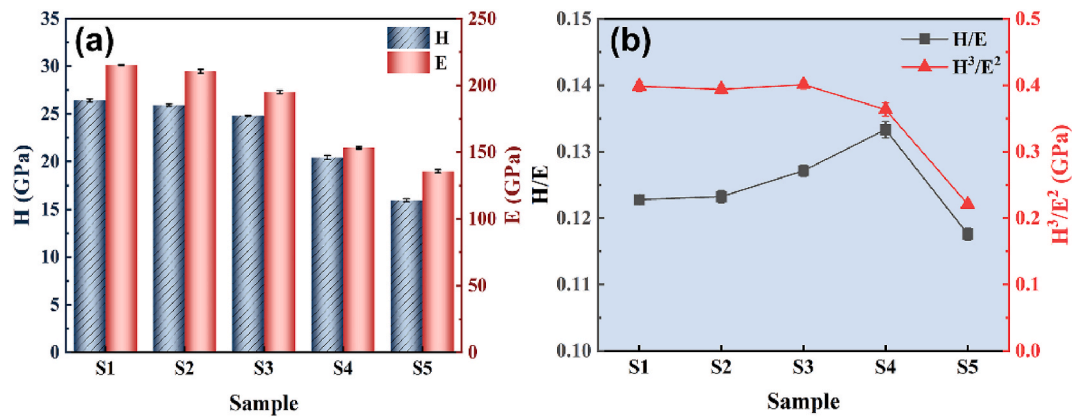

Fig. 6. (a) Hardness (H) and elastic modulus (E) and (b) H/E and H^3/E^2 of coatings. (Error bars represent the standard deviation. Data were collected from 6 measurements.)
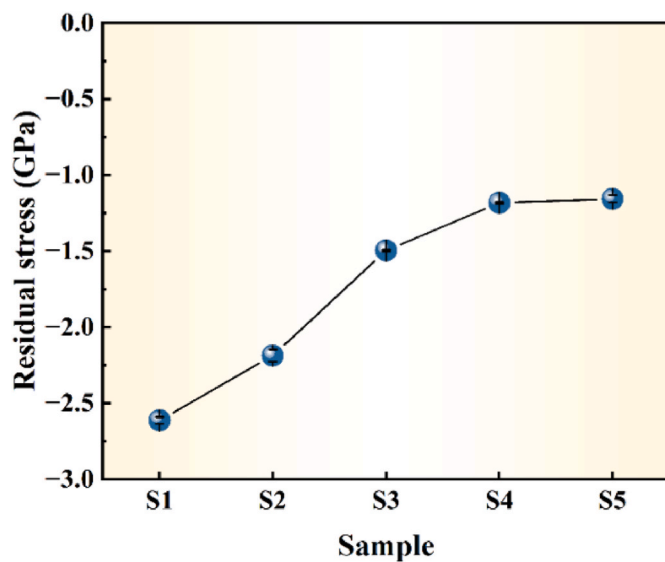

Fig. 7. Compressive residual stress of the single-layer coatings and a-C:H/a-C:H:Si:O FGCs. (Error bars represent the standard deviation. The data was collected from 3 measurements.)

adhesion strength, with a maximum pull-off force of approximately 577.3 N and an adhesion stress of 7.4 MPa. However, the maximum pull-off force between single-layer a-C:H coating and PEEK is only 250.7 N,

and the corresponding maximum adhesion stress is 3.2 MPa, indicating that Si and O co-doping significantly improves the adhesion strength.
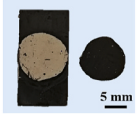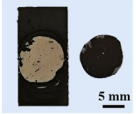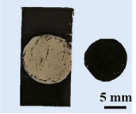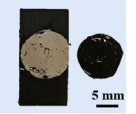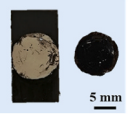
From the fracture morphology after pull-off tests, the coating is completely transferred to the surface of the cylindrical pin, and the PEEK is not damaged, indicating their adhesion failure characteristic. For functional gradient coatings, the adhesion stress gradually increases with the increase in the thickness ratio, which is consistent with the changing trend of the internal stress (Fig. 7). Generally, according to the research of Hu et al. [53], for amorphous carbon coatings, the residual stress is the dominant factor and is negatively correlated with its adhesion strength.

3.3. Tribological properties

Fig. 8(a) shows the friction coefficient (COF) curves for all coatings during the 60 min tribological test. The five samples exhibit various frictional states, which are related to their thickness ratio of a-C:H/a-C:H:Si:O. The initial COF of a-C:H coating (S1) is about 0.17 and increases slowly as the test time extends. After about 40 min, its COF increases sharply, indicating the failure of the coating. When the thickness ratio of a-C:H/a-C:H:Si:O reaches 9/1 (S2), its initial COF is 0.17 and increases slowly with test time without any dramatic fluctuation. For the S3 sample, its COF increases slowly and then decreases after 34 min, and then stabilizes at about 0.22 until the end of the test. The COF of S4 begins to decrease after 25 min and then remains stable after decreasing to approximately 0.1. When the friction test reaches 44.4 min, the COF increases sharply, indicating the failure of the coating. Obviously, a-C: H/a-C:H:Si:O FGCs significantly increase the wear life of the coated PEEK compared to single-layer amorphous carbon coatings.

Table 5
Maximum pull-off forces and stress and fracture types of the pull-off testing of the coatings (values in parentheses are standard deviations).

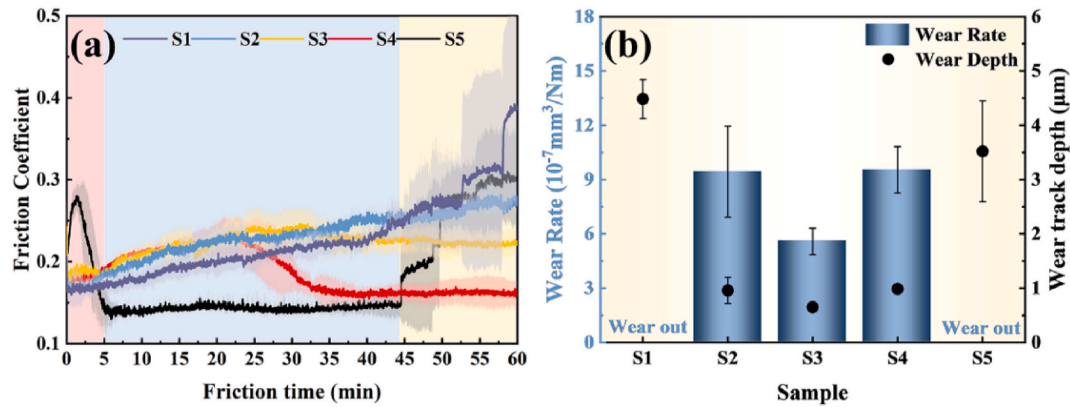| Sample	S1	S2	S3	S4	S5
Maximum pull-off force (N)	250.7 (9.3)	389.2 (67.3)	452.5 (100.6)	511.6 (113.8)	577.3 (174.6)
Maximum adhesion stress (MPa)	3.2 (0.1)	5.0 (0.9)	5.8 (1.3)	6.5 (1.5)	7.4 (2.2)
Fracture type	Adhesive at the PEEK/coating interface				
Fracture morphology					

Fig. 8. (a) Friction curves during the sliding process and (b) the wear rate and wear track depth of coatings after 1 h of tribological experiment. (Error bars represent the standard deviation. Data were collected from 3 samples.)
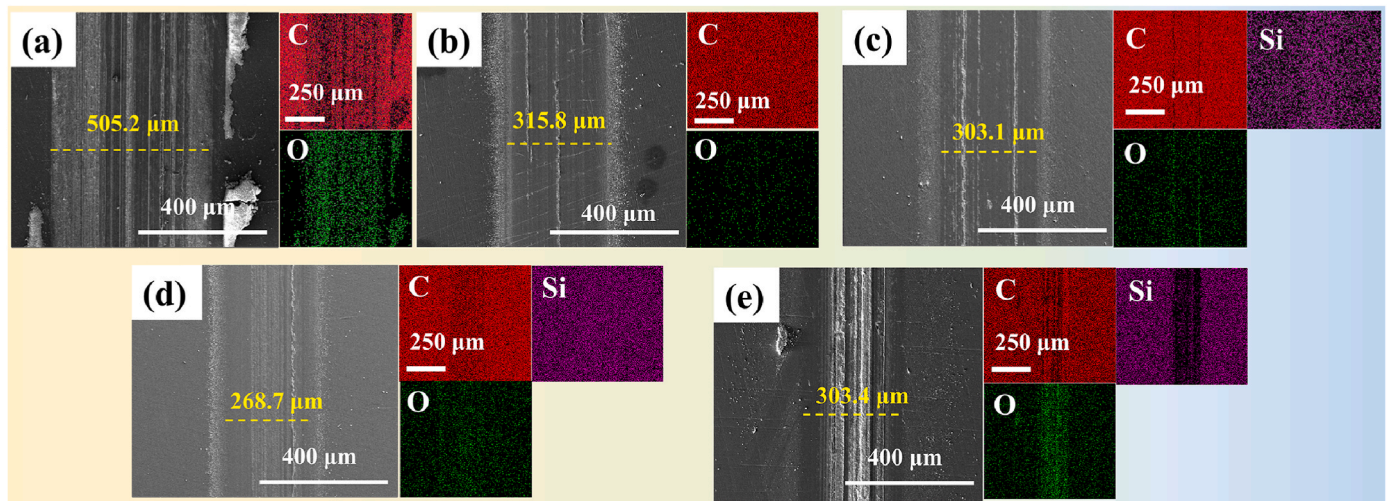
Fig. 9. The wear track of the coatings and the corresponding EDS mapping results from wear track: (a)~(e) corresponding S1~S5.

Fig. 8(b) shows the wear rate and the wear track depth after the tribological test. The wear rates of S2 to S4 coatings are 9.4, 5.6, and 9.5 $\times 10^{-7}$ mm^3/Nm respectively, and the corresponding wear depths are 0.96, 0.65, and 0.98 μm respectively, which are lower than the designed thickness of as-deposited coatings. In contrast, the samples with single-layer coating (S1 and S5) have the maximum wear depth range from 3.5 to 4.5 μm, indicating wear out of the coatings.

Fig. 9 shows surface morphology of wear tracks and corresponding EDS mapping results of coated PEEK. S1 has the widest wear track of 505.2 μm. The wear track widths of S2-S5 are 315.8 μm, 303.1 μm, 268.7 μm, and 303.4 μm respectively. According to the EDS mapping, there is no significant reduction of carbon and silicon contents in the wear track for S2 to S4. However, the C and Si elements in S1 and S5 are significantly reduced, while more O atoms are detected. Fig. 10 presents the Raman spectra of the wear track center for S1 and S5. The typical ether bonds (around 1146 cm^{-1}) and benzene rings (around 1508 cm^{-1}) confirm the exposure of PEEK substrate [34,54].

Fig. 11 shows the surface morphology and corresponding EDS energy spectra of wear scars from the mating balls. S1 sample exhibits the largest wear scars, with a diameter of 535.8 μm, and a considerable amount of wear debris is scatters around (Fig. 11(a)). The main constituents of the debris are C and O elements, which predominantly originate from the a-C:H coating. Virtually no C element is present in the center of the wear scars, signifying that no transfer film is formed. In contrast to S1, the quantity of debris accumulation around S2 to S4 is significantly diminished (Fig. 11(b–d)), and a strong C element signal
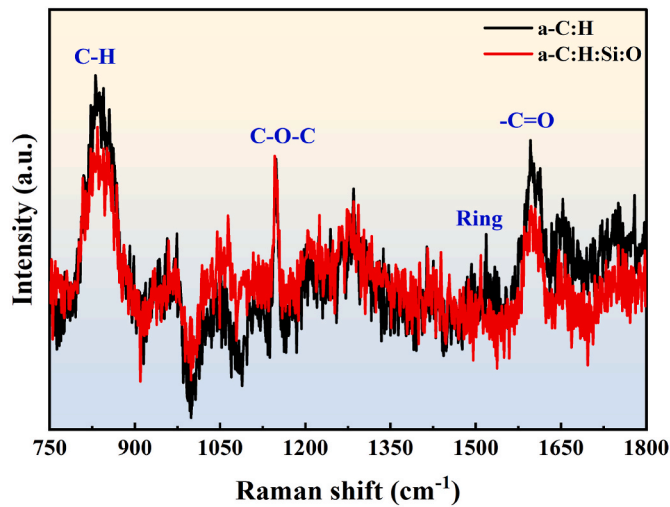
Fig. 10. The Raman spectra of wear track from S1 and S5.

still exists at the center of the wear scars, indicating that the transfer film is well retained. In the S4 sample, a robust Si element signal is observed, suggesting that the top a-C:H coating is worn out and the a-C:H:Si:O layer is exposed. In Fig. 11(e) for the S5 sample, the diameter of the scar is approximately 349.7 μm, and there is more wear debris around, which

retains a small quantity of the transfer film.

To gain a deeper understanding of the friction process of the coatings, the tribological behaviors at the initial stage (the first 3 min) and the stable stage (25 min) are investigated. In Fig. 12(a), the samples featuring the top a-C:H layer (S1 ~ S4) have a relatively higher wear rate ranging from 1.9 to 3.7 × 10^{-7} mm^3/Nm at the initial stage. Their wear rate decreases significantly in the stable stage, and the S3 demonstrates the lowest wear rate of 1.3 × 10^{-7} mm^3/Nm and 0.4 × 10^{-7} mm^3/Nm at 3 and 25 min, respectively. Regarding the single-layer a-C:H:Si:O coating (S5), its wear rate at the initial stage is marginally higher than that at the stable stage, which are 1.2 × 10^{-7} mm^3/Nm and 1.5 × 10^{-7} mm^3/Nm, respectively. From the wear depth of the different stages in Fig. 12(b), the wear depth of all samples at 3 min and 25 min is considerably less than the thickness of the five coatings, indicating that the coatings are still capable of protecting the PEEK substrate. The S2 has the greatest wear depth of 0.41 μm, while S3 and S5 have the smallest wear depth of 0.07 μm at the initial stage. At 25 min, the wear track depth for each sample is greater than that at 3 min, the wear depth of S4 and S5 increases sharply to 0.57 and 0.63 μm, respectively, indicating that the coating has undergone severe wear. However, S3 still has the slightest wear track depth of 0.16 μm. For all samples, their wear track depths reach the peak value when the friction test duration is extended to 60 min. For the single-layer coatings, the a-C:H (S1) and a-C:H:Si:O (S5) coated PEEK exhibits significantly aggravated wear, with wear track depths of 4.5 μm and 3.5 μm, respectively. These values are well above the wear depths observed at the 25-min mark and
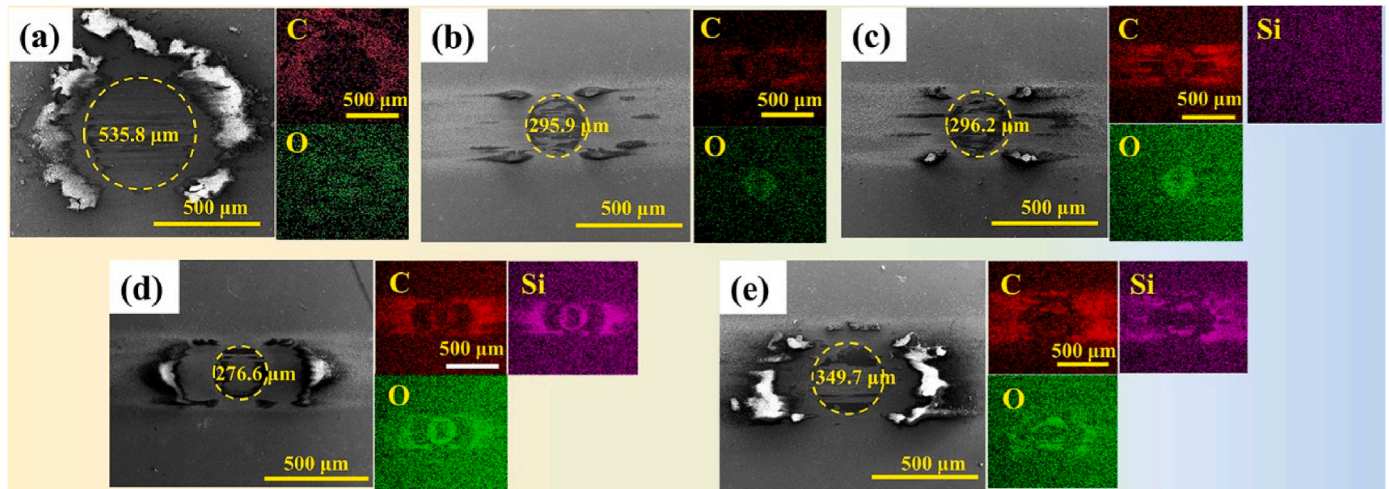
Fig. 11. Surface morphologies and EDS energy spectra of the wear scars: (a) ~ (e) corresponding S1 ~ S5.
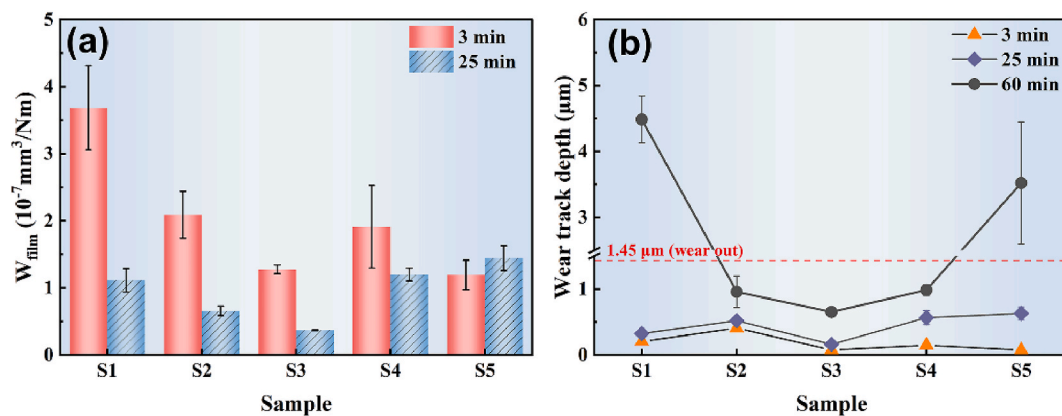
Fig. 12. (a) Wear rate and (b) wear track depth of coatings after 3 min and 25 min tribological test. (Error bars represent the standard deviation. Data were collected from 3 samples.)
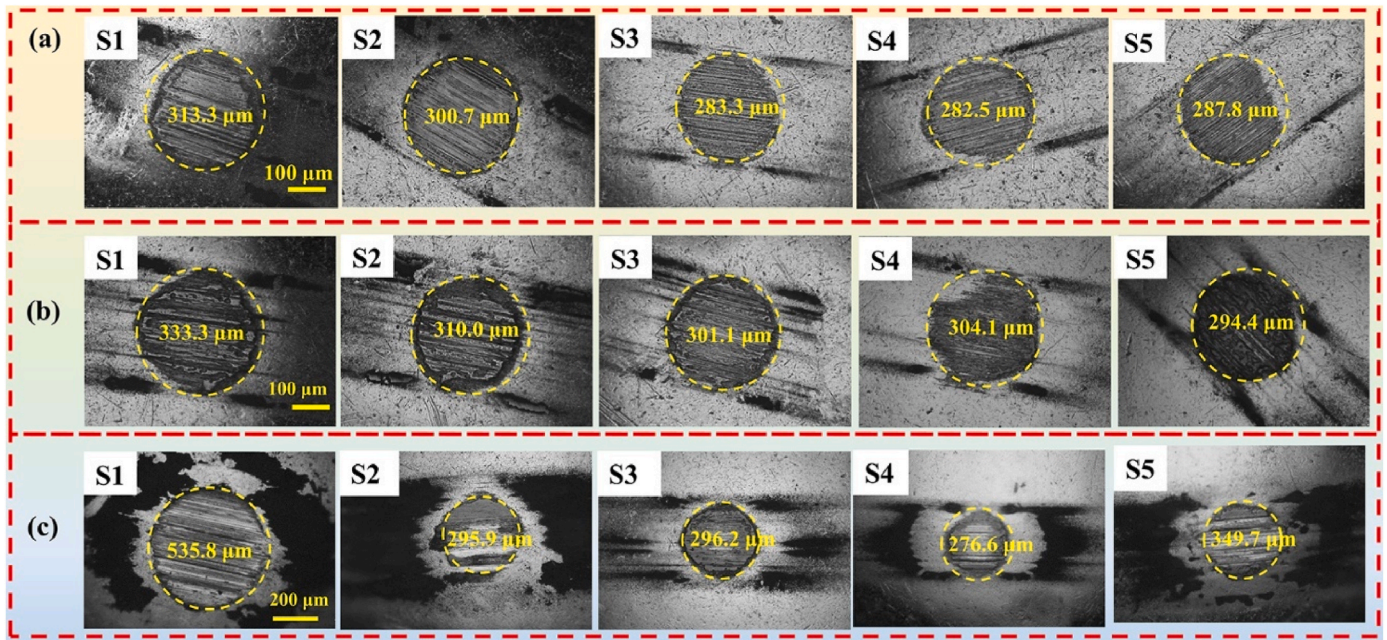
Fig. 13. The morphologies of wear scars on the matting ball in different friction periods, (a) initial stage (friction for 3 min), (b) stable stage (friction for 25 min), and (c) later or failed stage (friction for 60 min).
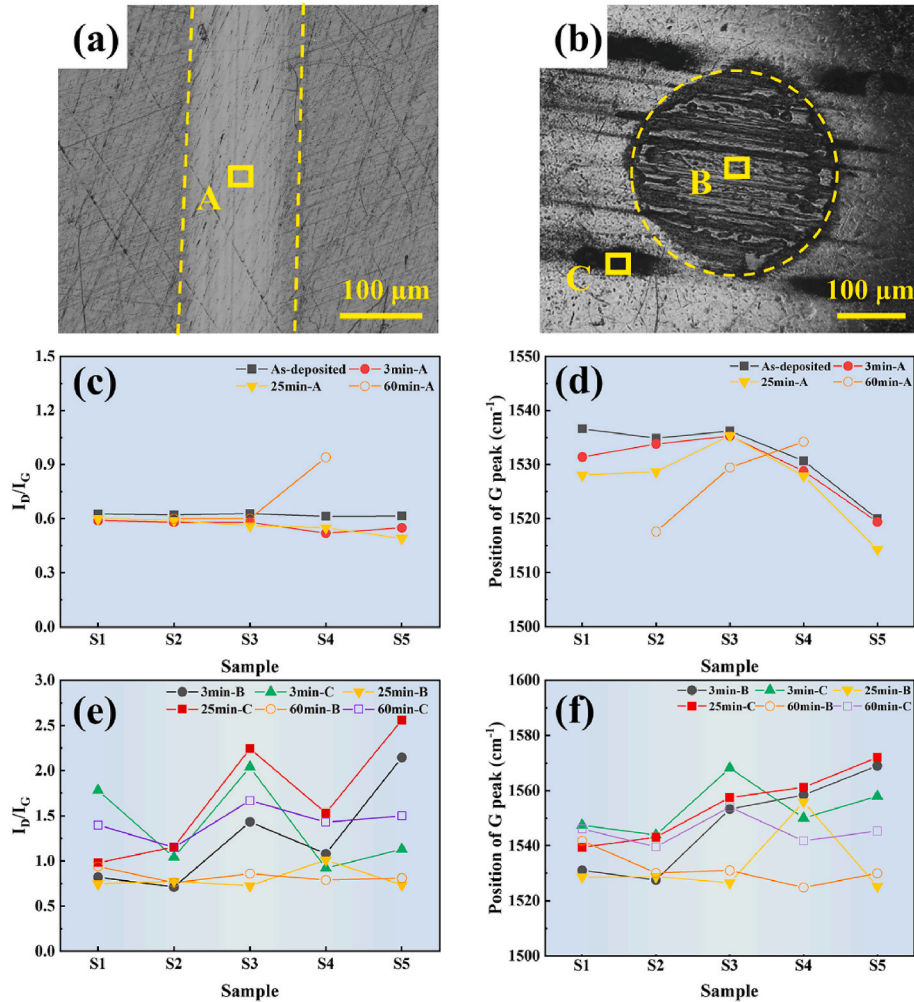
Fig. 14. (a, b) Raman test for wear tracks and wear scars, and (c) ~ (f) the corresponding fitting results.

Fig. 15. Equivalent stress contours for (a) a-C:H coated PEEK, (b) a-C:H:Si:O coated PEEK, (c) a-C:H/a-C:H:Si:O FGC coated PEEK. Regions A, B, and C are the magnified view of the contact center of the model, the position of maximum stress and the stress contours of the coating, respectively.

significantly greater than the original coating thickness. In contrast, the FGCs samples maintain structural integrity at the 60-min stage, among which the S3 exhibits the lowest wear track depth. Notably, compared to the friction stable stage (3–25 min), the increase in wear track depth duri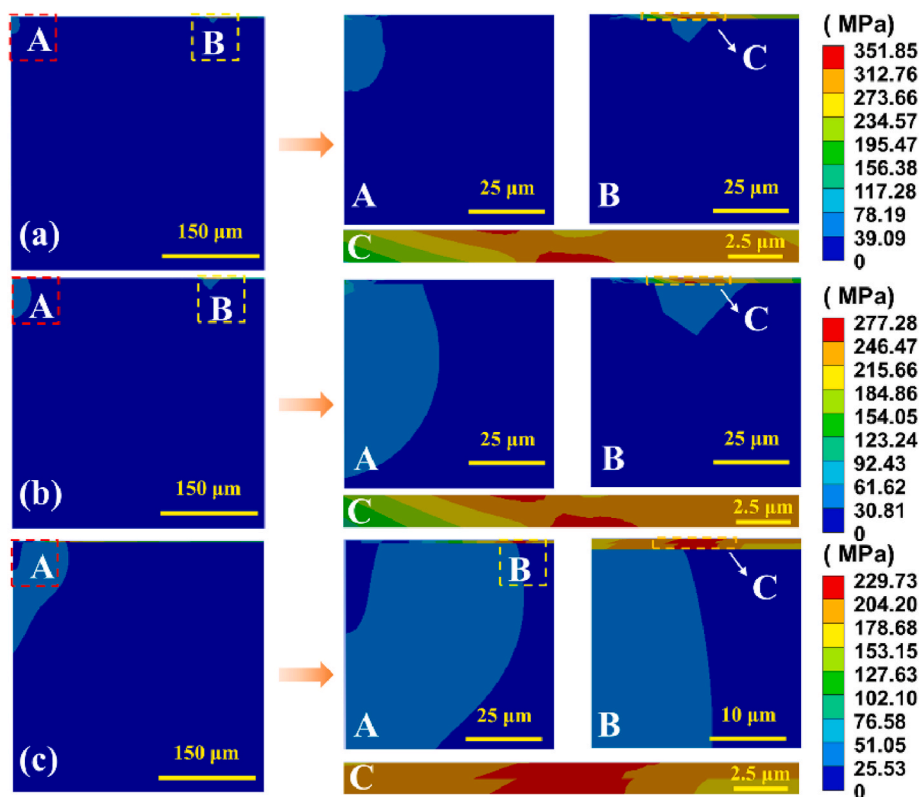ng the later stage (25–60 min) becomes more pronounced, indicating a characteristic of accelerated wear. Overall, the FGCs samples demonstrate significantly superior wear resistance compared to single-layer coatings, with the optimal wear performance under gradient ratio of 1:1 (as seen in S3).

The morphologies of the wear scars on matting balls at various friction stages are analyzed in detail as well. In Fig. 13, circular wear scars emerge on the matting ball at different friction stages, with many parallel grooves arranged along the sliding direction. During the running-in period in Fig. 13(a) and stable period in Fig. 13(b), a significantly greater amount of black substances are transferred from the coating to the matting ball, and the diameter of the wear scar also enlarges. At 60 min, the wear debris around the wear scar of all samples increases dramatically, as shown in Fig. 13(c). The wear scar diameter of S1 and S5 increases by 61 % and 19 %, respectively, compared to that during the stable period. While contrary to the single-layer coatings, all the FGCs display a smaller wear scar, owing to the formed transfer film.

The structural alteration of the coating during the sliding process is another crucial factor influencing its tribological properties. Three typical areas of the wear tracks and wear scars (Fig. 14(a and b)) are examined by Raman, where A denotes the center of the wear track, B represents the center of the wear scar, and C indicates the area around the wear scar with scattered debris.

For the as-deposited coatings, they possess similar sp^2-C cluster sizes, and their C-sp^3 content exhibits an ascending trend when the coatings are doped with Si and O elements. According to Fig. 14(c, d) from area A, the I_D/I_G and G peak positions after 3 and 25 min are lower than that of the as-deposited coating, signifying that the sp^2-C cluster size reduces and the sp^3 content increases after the friction test. After 1 h test,

characteristic peaks of amorphous carbon could not be detected for S1 and S5, indicating the failure of the two single-layer coatings. In S2 and S3, the I_D/I_G value and G peak position are still lower than that of the as-deposited coating. However, the I_D/I_G value and G peak position of S4 increase to 0.9 and 1534.2 cm^{-1}, respectively, which are significantly higher than the as-deposited coating, indicating severe graphitization on the wear track.

The B area can reflect the evolution of transfer film or tribo-film. In Fig. 14(e and f), the I_D/I_G value and G peak position of the transfer materials on the mating ball are notably higher than those on the wear tracks, which confirms the formation of a graphitized transfer layer. In the initial stage (3 min), samples with a thicker a-C:H:Si:O layer, such as S3-S5, have greater value of I_D/I_G and G peak positions, indicating that these materials transferred from the coating to the mating ball have a larger sp^2-C cluster size and more sp^2-C content at this stage. In the stable and the subsequent stages (25 and 60 min), the I_D/I_G values at area B are comparable for all samples. However, at 25 min, the G peak position of the transfer layer in S4 is significantly larger than that for other samples, indicating its highest sp^2-C content. Although the S5 fails after 60 min, the residual transfer material on the mating ball still has similar I_D/I_G and G peak positions close to that of the S4, indicating a similar graphitization process before its failure.

At the C area, the I_D/I_G and G peak positions of the wear debris are greater than those of the transfer layer in the stable and later stages, which indicates that the wear debris is formed through the graphitization of the transfer layer in the friction test. Additionally, for the two single-layer coatings, the changes in their I_D/I_G and G peak position value are within a wide range throughout the entire friction test. Meanwhile, the FGCs exhibit relatively stable structure characteristics, especially for the S3 sample, its I_D/I_G and G peak position values are nearly the same.
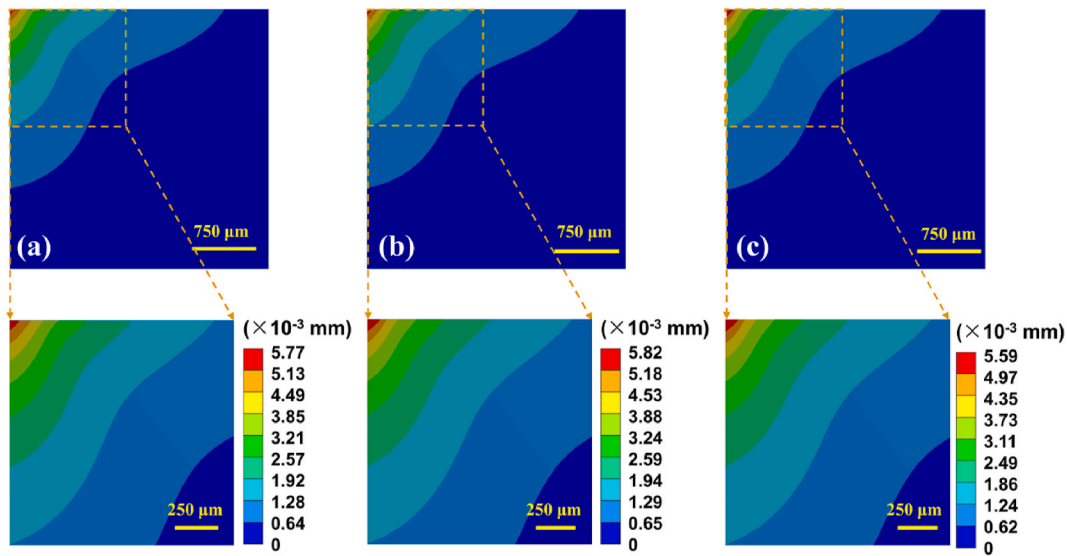
Fig. 16. Deformation contours for (a) a-C:H coated PEEK, (b) a-C:H:Si:O coated PEEK, (c) a-C:H/a-C:H:Si:O FGC coated PEEK.

3.4. Stress distribution and deformation of the system

During the friction test, a normal applied load will induce stress and deformation in coated PEEK. Analyzing the stress distribution and deformation characteristics of coated PEEK is beneficial for explaining their tribological behaviors. The distribution contour of the equivalent stress from different systems is shown in Fig. 15. The equivalent von Mises stress within the coating results mainly from the normal load and the elastic modulus mismatch. High stresses due to normal loads are concentrated below the contact area, while stresses from elastic modulus mismatch occur mainly at the interface [55,56]. In this study, the stress concentration appears at the center of the contact region (region A) between the ball and the sample. Further analysis reveals a distinct geometric transition in region B when the sample deformation is magnified five times (Fig. S3) This geometric transition is caused by the mismatch in the elastic modulus between coatings and PEEK under external loading. As a result, stress distortion at this transition leads to localized high stress concentration. The von Mises stress distribution field of the single-layer coating system is similar (Fig. 15(a and b)), the maximum stress value appears at the upper surface of the coating and the coating-substrate interface, which is in accordance with the stress distribution of hard coatings reported in the literature [57,58]. The maximum stresses of a-C:H coated PEEK and a-C:H:Si:O coated PEEK are 351.85 and 277.28 MPa, respectively. Whereas the stress distribution in the FGC system is different, the maximum stress is uniformly distributed along the thickness of the coating, the lowest value of their maximum stress is only 229.73 MPa (Fig. 15(c)). Further, regions A, B, and C are respectively the magnified view of the contact center of the model, the position of maximum stress, and the stress contours of the coating. The maximum stress in the three systems is far away from the contact center of the model. The stress distribution profiles of the single-layer coatings are similar, and there is obvious stress concentration on the upper surface of the coating and the coating-substrate interface. However, the red region of the maximum stress in the FGC is uniformly distributed in the thickness direction, indicating that the stress release in the FGC is superior to that in the single-layer coating.

Fig. 16 presents the deformation from different systems. The deformation profiles of all coating systems are identical. The maximum deformation occurs at the center of contact between the ball and the coating and decreases gradually as the distance from the contact center increases. However, there are significant differences in the maximum deformation values of the three systems. The maximum deformations of the a-C:H coated PEEK, a-C:H:Si:O coated PEEK, and FGC coated PEEK

are 5.77, 5.82, and 5.59 $\times$ 10^{-3} mm respectively.

4. Discussion

The FGC coated PEEK demonstrates superior wear resistance compared to the single-layer amorphous carbon coated one. At least three aspects should be considered to uncover the underlying wear mechanism, including the stress distribution and deformation characteristics, formation of the transfer film, chemical structure changes during the tribological test.

For a-C:H coated PEEK, the fundamental premise of its enhanced tribological performance lies in the existence of a-C:H or carbon-based transfer film in the sliding interface. Obviously, the early spalling of the two single-layer coatings led to a lack of lubricating material and their poor protective performance.

The priority is to analyze their stress distribution and deformation characteristics. From the finite element method model, there is conspicuous stress concentration in the single-layer coated PEEK, which is the main cause of cracks in the coating [59,60]. Besides, the maximum stress value emerges at the interface between the coatings and the PEEK substrate and all coatings show adhesion failure characteristics (Table 5). However, the FGCs show reduced stress concentration, with a maximum stress decline of 35 % (Fig. 15). The single-layer a-C:H coated PEEK has the lowest adhesion strength, so numerous cracks are produced on the surface of single-layer a-C:H coated PEEK during friction test [27]. Additionally, according to GD-OES and XPS depth profiles, the FGCs avoid the composition mutation from the PEEK to the a-C:H coating, which endows the FGCs coated PEEK with better plastic deformation resistance and mechanical stability [30,61,62]. As a result, FGCs coated PEEK can hold the stress concentration and deformation during tribological tests without obvious spalling, demonstrating their better protective performance.

The second aspect is that once the carbon-based coatings cover the PEEK during the tribological test, their tribological performance is highly dependent on the transfer film [63–65]. In the initial stage (the first 3 min), a small amount of transfer material is observed on the mating balls of all samples (Fig. 13(a)). From the initial stage (3 min) to the stable stage (25 min), the transfer material on the mating ball increases and forms a complete transfer film (Fig. 13(b)), resulting in a reduced wear rate of the coatings. At the later stage of friction (60 min), the diameter of the wear scar on the mating ball for single-layer coated PEEK increases significantly, and the corresponding transfer film is consumed (Fig. 13 (c)), indicating that the single-layer coatings cannot
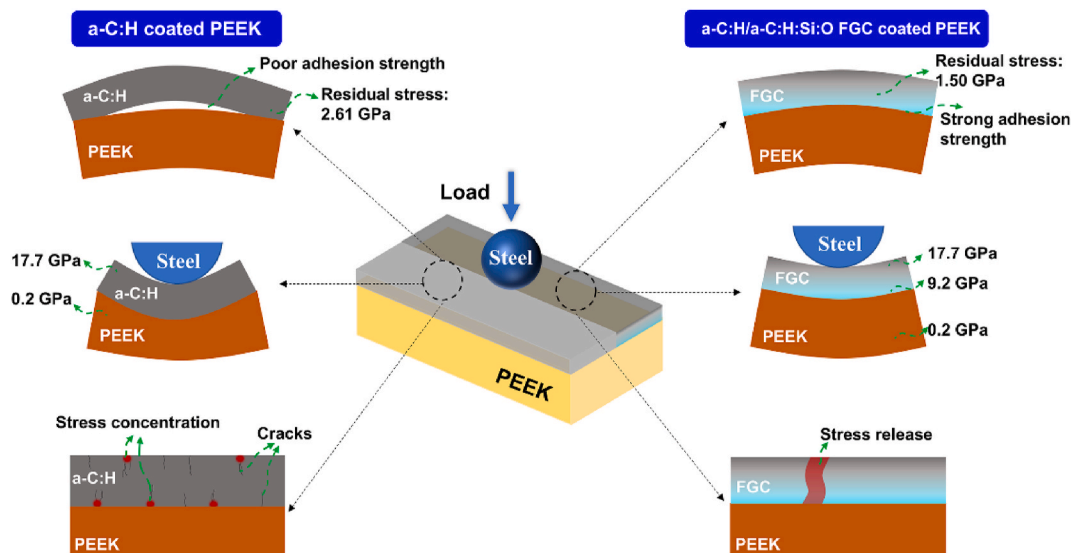
Fig. 17. Schematic illustration of tribological failure mechanism for single-layer a-C:H coated PEEK and a-C:H/a-C:H:Si:O FGC coated PEEK.

provide long-term protection for PEEK. However, for all the FGCs samples, their mating balls show a smaller wear scar, due to the dense transfer film on their surface.

A final factor is the chemical structure change during the tribological test. Among the FGCs coatings, the interaction between the wear track and the transfer film determines their COF and wear rate. After 1 h of tribological test, the wear track depth of S2 is less than the thickness of the top a-C:H layer, and the wear track depths of S3 and S4 are much larger than the top a-C:H thickness (Fig. 8(b)), so fewer Si and O atoms will be involved in the tribo-chemical reaction for S2. Since Si and O atoms are beneficial for the graphitization of C-sp^3 under the friction test [66], the sp^2-C content in the wear track from high to low in turn is S4, S3, S2, as affirmed by Raman spectra (Fig. 14(c)). During the tribological test, more C-sp^3 in the wear track causes more covalent bonds with the transfer film on the matting ball, which requires more tensile force to break [42], so S2 has the highest COF and a higher wear rate. S4 has the lowest friction coefficient, however, its poor mechanical properties and deformation resistance (Fig. 6) also account for its relatively highest wear rate. Overall, S3 has the optimum gradient structure, this appropriate thickness ratio of a-C:H to a-C:H:Si:O implies both excellent mechanical properties and lubricating properties, resulting in its best tribological performance.

Based on the mentioned analysis, the tribological failure mechanism of FGC coated PEEK is proposed, as shown in Fig. 17. For the single-layer a-C:H coating, its high compressive residual stress and weak interfacial adhesion strength can result in early spalling of the coating, and the following lack of lubricating material in the sliding interface can cause its poor wear resistance. In contrast, by incorporating the a-C:H:Si:O transition layer between a-C:H and PEEK, the FGCs samples have both reduced residual stress and higher adhesion strength, so the less spalling of the FGCs coating and more dense transfer film during tribological test provide its superior wear resistance.

5. Conclusion

By introducing a gradient composition of Si and O into the interface, the a-C:H/a-C:H:Si:O FGCs are prepared on PEEK. The effects of the structure of a-C:H/a-C:H:Si:O FGC on its mechanical properties and tribological behaviors are systematically investigated, and the wear mechanisms of the coatings were elucidated. The following conclusions can be drawn:

1. The residual stress and adhesion strength of a-C:H/a-C:H:Si:O FGCs are greatly governed by its thickness ratio. With the increase in thickness of a-C:H:Si:O, the residual stress of FGCs gradually decreases, the adhesion strength between the amorphous carbon coatings and PEEK increases from 3.2 MPa to 6.5 MPa.
2. Compared with the single-layer a-C:H:Si:O and a-C:H, FGCs coated PEEK has higher H and E and an appropriate element transition zone, resulting in its excellent deformation resistance. PEEK coated with FGCs also shows reduced stress concentration, with a maximum stress decline of 35 %.
3. PEEK coated with FGCs exhibits superior tribological performance compared to single-layer coatings. With the optimum thickness ratios of a-C:H and a-C:H:Si:O (1/1), S3 can avoid stress concentration and maintain excellent mechanical and lubricating properties, which accounts for its best wear resistance and a minimum wear rate of 5.6 $\times 10^{-7}$ mm^3/Nm.

CRediT authorship contribution statement

Xianchun Jiang: Writing – review & editing, Writing – original draft, Software, Data curation. **Lingkang Meng:** Software, Data curation. **Peng Guo:** Writing – review & editing, Funding acquisition, Conceptualization. **Rende Chen:** Investigation. **Zhenyu Wang:** Data curation. **Hao Li:** Data curation. **Kazuhito Nishimura:** Writing – review & editing, Funding acquisition. **Aiying Wang:** Writing – review & editing, Supervision, Funding acquisition. **Peiling Ke:** Writing – review & editing, Supervision, Project administration, Funding acquisition, Conceptualization.

Declaration of competing interest

The authors declare that they have no known competing financial interests or personal relationships that could have appeared to influence the work reported in this paper.

Appendix ASupplementary data

Supplementary data to this article can be found online at https://doi.org/10.1016/j.wear.2025.206326.

Data availability

Data will be made available on request.

References

[1] B. Cheng, H. Duan, Q. Chen, H. Shang, Y. Zhang, J. Li, T. Shao, Effect of laser treatment on the tribological performance of polyetheretherketone (PEEK) under seawater lubrication, Appl. Surf. Sci. 566 (2021) 150668, https://doi.org/10.1016/j.apsusc.2021.150668.

[2] H.X. Lyu, N.Y. Jiang, Y.Z. Li, D.X. Zhang, Enhancing CF/PEEK interfacial adhesion by modified PEEK grafted with carbon nanotubes, Compos. Sci. Technol. 210 (2021) 108831, https://doi.org/10.1016/j.compscitech.2021.108831.

[3] S. Zhang, F. Awaja, N. James, D.R. McKenzie, A.J. Ruys, Autohesion of plasma treated semi-crystalline PEEK: comparative study of argon, nitrogen and oxygen treatments, Colloids Surf., A 374 (2011) 88–95, https://doi.org/10.1016/j.colsurfa.2010.11.013.

[4] C. Feng, Y. Guo, Z. Yu, K. Chen, D. Wang, X. Li, Y. Luo, Q. Wang, D. Zhang, Tribological properties of PEEK composites reinforced by MoS2 modified carbon fiber and nano SiO2, Tribol. Int. 181 (2023) 108315, https://doi.org/10.1016/j.triboint.2023.108315.

[5] T.N. Ren, G.M. Zhu, C.S. Zhang, S.Y. Wang, Preparation of CF/PEEK composites with high mechanical performance using PEEK derivatives as the sizing agent, Macromol. Rapid Commun. 44 (2023) 2200738, https://doi.org/10.1002/marc.202200738.

[6] P. Shetty, P. Dsilva, P. Sondar, B.G. Kumar, S. Hegde, Biodegradation of PEEK piston rings, Polym. Degrad. Stabil. 191 (2021) 109666, https://doi.org/10.1016/j.polymdegradstab.2021.109666.

[7] Z. Zheng, P.J. Liu, X.M. Zhang, J.G. Xin, Y.J. Wang, X.S. Zou, X.H. Mei, S.L. Zhang, S.K. Zhang, Strategies to improve bioactive and antibacterial properties of polyetheretherketone (PEEK) for use as orthopedic implants, Mater. Today Bio 16 (2022) 100402, https://doi.org/10.1016/j.mtbio.2022.100402.

[8] D. Li, Y. Liu, Y. Deng, M. Fang, D. Wu, The effect of different temperatures on friction and wear properties of CFRPEEK against AISI 431 steel under water lubrication, Tribol. Trans. 61 (2017) 357–366, https://doi.org/10.1080/10402004.2017.1326649.

[9] Y. Ran, Q. He, W.F. Huang, Y. Liu, Y.M. Wang, Analysis of the coupling mechanism of the dynamic response and mechanical-thermal deformation in mechanical seals, Tribol. Int. 192 (2024) 109257, https://doi.org/10.1016/j.triboint.2024.109257.

[10] R. Gong, M. Liu, H. Zhang, Y. Xu, Experimental investigation on frictional behavior and sealing performance of different composites for seal application, Wear 342 (2015) 334–339, https://doi.org/10.1016/j.wear.2015.10.001.

[11] A. Maslavi, H. Unal, M.N. Olabi, Determination of "tribological performance working fields" for pure PEEK and PEEK composites under dry sliding conditions, Wear 554–555 (2024) 205464, https://doi.org/10.1016/j.wear.2024.205464.

[12] Z. Guan, D. Wu, Q. Cheng, Z. Wang, M. Tang, Y. Liu, Friction and wear characteristics of CF/PEEK against 431 stainless steel under high hydrostatic pressure water lubrication, Mater. Des. 196 (2020) 109057, https://doi.org/10.1016/j.matdes.2020.109057.

[13] N. Dhakal, C. Espejo, A. Morina, N. Emami, Tribological performance of 3D printed neat and carbon fiber reinforced PEEK composites, Tribol. Int. 193 (2024) 109356, https://doi.org/10.1016/j.triboint.2024.109356.

[14] L.L. Xue, Q.Q. Xu, C.H. Meng, S.Y. Lei, G.D. Zhang, M.X. Tang, W.R. Zhai, H. Yu, X. Q. Liu, C.F. Du, Achieving the ultra-low friction and wear rate of PEEK-PTFE composites by Ti3C2Tx MXene reinforcement, Tribol. Int. 199 (2024) 110030, https://doi.org/10.1016/j.triboint.2024.110030.

[15] A.H. Mir, M.S. Charoo, Friction and wear characteristics of polyetheretherketone (PEEK)-A review, Mater. Sci. Eng. 561 (2019) 012051, https://doi.org/10.1088/1757-899X/561/1/012051.

[16] Y. Yan, C. Jiang, Y. Huo, C. Li, Preparation and tribological behaviors of lubrication-enhanced PEEK composites, Appl. Sci. 10 (2020) 7536, https://doi.org/10.3390/app10217536.

[17] Z. Wang, C. Wang, Y. Zhang, A. Wang, P. Ke, M-site solid solution of vanadium enables the promising mechanical and high-temperature tribological properties of Cr2AlC coating, Mater. Des. 222 (2022) 111060, https://doi.org/10.1016/j.matdes.2022.111060.

[18] R.-N. Ji, C.-X. Liu, J. Zhang, S.-G. Zhang, L. Zhang, Y. Lian, Hydrophobicity and tribological properties of Al2O3/PTFE composite coating, Rare Met. 42 (2018) 3870–3876, https://doi.org/10.1007/s12598-018-1149-0.

[19] S. Urdem, E. Duru, H. Algul, M. Uysal, H. Akbulut, Evaluation of high temperature tribological behavior of electroless deposited NiB-Al(2)O(3)coating, Wear 482 (2021) 203960, https://doi.org/10.1016/j.wear.2021.203960.

[20] M. Ueda, A. Kadiric, H. Spikes, Wear of hydrogenated DLC in MoDTC-containing oils, Wear 474 (2021) 203869, https://doi.org/10.1016/j.wear.2021.203869.

[21] J. Yao, F. Yan, Y. Yang, H. Chen, B. Chen, L. Zhu, B. Long, M. Yan, Y. Zhang, On the growth of functionally graded self-lubricating layer during a plasma-assisted thermochemical treatment of M50NiL steel, Appl. Surf. Sci. 584 (2022) 152517, https://doi.org/10.1016/j.apsusc.2022.152517.

[22] R. Zhao, J. Steiner, K. Andreas, M. Merklein, S. Tremmel, Investigation of tribological behaviour of a-C:H coatings for dry deep drawing of aluminium alloys, Tribol. Int. 118 (2018) 484–490, https://doi.org/10.1016/j.triboint.2017.05.031.

[23] J.P. Sullivan, T.A. Friedmann, A.G. Baca, Stress relaxation and thermal evolution of film properties in amorphous carbon, J. Electron. Mater. 26 (1997) 1021–1029, https://doi.org/10.1007/s11664-997-0239-9.

[24] P.M. Yin, X.B. Wei, L.L. Shang, Z.B. Lu, G.A. Zhang, Design of low-friction and anti-corrosion a-C:H:SiOx films, Diam. Relat. Mater. 118 (2021) 108512, https://doi.org/10.1016/j.diamond.2021.108512.

[25] L. Li, W. Song, J. Liu, Q. Liu, S. Wang, G. Zhang, Nanomechanical and nanotribological behavior of ultra-thin silicon-doped diamond-like carbon films, Tribol. Int. 94 (2016) 616–623, https://doi.org/10.1016/j.triboint.2015.10.026.

[26] D. Zhang, S. Li, X. Zuo, P. Guo, P. Ke, A. Wang, Structural and mechanism study on enhanced thermal stability of hydrogenated diamond-like carbon films doped with Si/O, Diam. Relat. Mater. 108 (2020) 107923, https://doi.org/10.1016/j.diamond.2020.107923.

[27] X. Jiang, P. Guo, L. Cui, Y. Zhang, R. Chen, Y. Ye, A. Wang, P. Ke, Tribological behavior of silicon and oxygen co-doped hydrogenated amorphous carbon coatings on polyether ether ketone, Diam. Relat. Mater. 132 (2023) 109650, https://doi.org/10.1016/j.diamond.2022.109650.

[28] D. Wu, J. Shi, F. Niu, G. Ma, C. Zhou, B. Zhang, Direct additive manufacturing of melt growth Al2O3-ZrO2 functionally graded ceramics by laser directed energy deposition, J. Eur. Ceram. Soc. 42 (2022) 2957–2973, https://doi.org/10.1016/j.jeurceramsoc.2022.01.034.

[29] V.B. Zelentsov, P.A. Lapina, B.I. Mitrin, Wear of functionally graded coatings under frictional heating conditions, Nanomaterials-Basel 12 (2022) 142, https://doi.org/10.3390/nano12010142.

[30] Z.Z. Wang, K. Wang, H.B. Huang, X. Cui, X.M. Shi, X.Q. Ma, B. Li, Z.Q. Zhang, X. H. Tang, M.Y.M. Chiang, Bioinspired wear-resistant and ultradurable functional gradient coatings, Small 14 (2018) 1802717, https://doi.org/10.1002/smll.201802717.

[31] G.J. Xu, M. Kutsuna, Z.J. Liu, L.Q. Sun, Characteristic behaviours of clad layer by a multi-layer laser cladding with powder mixture of Stellite-6 and tungsten carbide, Surf. Coating. Technol. 201 (2006) 3385–3392, https://doi.org/10.1016/j.surfcoat.2006.07.210.

[32] S. Banthia, S. Sengupta, S. Das, K. Das, Cu, Cu-SiC functionally graded coating for protection against corrosion and wear, Surf. Coating. Technol. 374 (2019) 833–844, https://doi.org/10.1016/j.surfcoat.2019.06.050.

[33] Z.K. Weng, A.H. Wang, X.H. Wu, Y.Y. Wang, Z.X. Yang, Wear resistance of diode laser-clad Ni/WC composite coatings at different temperatures, Surf. Coating. Technol. 304 (2016) 283–292, https://doi.org/10.1016/j.surfcoat.2016.06.081.

[34] X. Zhou, Y. Zhang, P. Guo, L. Cui, A. Wang, P. Ke, Tribological behavior of Cr/a-C multilayered coating against PEEK under dry sliding condition, Wear 518–519 (2023) 204625, https://doi.org/10.1016/j.wear.2023.204625.

[35] W.C. Oliver, G.M. Pharr, An improved technique for determining hardness and elastic modulus using load and displacement sensing indentation experiments, J. Mater. Res. 7 (2011) 1564–1583, https://doi.org/10.1557/jmr.1992.1564.

[36] J. Kovac, J. Ekar, M. Cekada, L. Zajickova, D. Necas, L. Blahova, J.Y. Wang, M. Mozetic, Depth profiling of thin plasma-polymerized amine films using GDOES in an Ar-O-2 plasma, Appl. Surf. Sci. 581 (2022) 152292, https://doi.org/10.1016/j.apsusc.2021.152292.

[37] J. Laconte, F. Iker, S. Jorez, N. Andre, J. Proost, T. Pardoen, D. Flandre, J.P. Raskin, Thin films stress extraction using micromachined structures and wafer curvature measurements, Microelectron. Eng. 76 (2004) 219–226, https://doi.org/10.1016/j.mee.2004.07.003.

[38] J. Dufils, F. Faverjon, C. Héau, C. Donnet, S. Benayoun, S. Valette, Combination of laser surface texturing and DLC coating on PEEK for enhanced tribological properties, Surf. Coating. Technol. 329 (2017) 29–41, https://doi.org/10.1016/j.surfcoat.2017.09.028.

[39] A. Esfarjani, M.M. Shokrieh, Effects of TiO2 nanoparticles and silane coupling agents on the adhesion strength and weathering properties of silicone rubber coatings, Int. J. Adhesion Adhes. 130 (2024) 103604, https://doi.org/10.1016/j.ijadhadh.2023.103604.

[40] G. Theiler, T. Gradt, Influence of counterface and environment on the tribological behaviour of polymer materials, Polym. Test. 93 (2021) 106912, https://doi.org/10.1016/j.polymertesting.2020.106912.

[41] F.D. Rzatki, D.V.D. Barboza, R.M. Schroeder, G.M.D. Barra, C. Binder, A.N. Klein, J. D.B. De Mello, Effect of temperature and atmosphere on the tribological behavior of a polyether ether ketone composite, Friction 3 (2015) 259–265, https://doi.org/10.1007/s40544-015-0091-5.

[42] J.H. Liang, Z. Milne, M. Rouhani, Y.-P. Lin, R.A. Bernal, T. Sato, R.W. Carpick, Y. R. Jeng, Stress-dependent adhesion and sliding-induced nanoscale wear of diamond-like carbon studied using in situ TEM nanoindentation, Carbon 193 (2022) 230–241, https://doi.org/10.1016/j.carbon.2022.03.030.

[43] Y. Su, Y. Wang, C. Wang, J. Li, W. Guan, W. Guo, Y. Sui, J. Lan, In-situ growing amorphous carbon film with attractive mechanical and tribological adaptability on PEEK via continuous plasma-induced process, Vacuum 187 (2021) 110147, https://doi.org/10.1016/j.vacuum.2021.110147.

[44] H. Sun, F. Lei, T. Li, H. Han, B. Li, D. Li, D. Sun, Facile fabrication of novel multifunctional lubricant-infused surfaces with exceptional tribological and anticorrosive properties, ACS Appl. Mater. Interfaces 13 (2021) 6678–6687, https://doi.org/10.1021/acsami.0c21667.

[45] S. Davey, R. Das, W.J. Cantwell, S. Kalyanasundaram, Forming studies of carbon fibre composite sheets in dome forming processes, Compos. Struct. 97 (2013) 310–316, https://doi.org/10.1016/j.compstruct.2012.10.026.

[46] M.F. Arif, H. Alhashmi, K.M. Varadarajan, J.H. Koo, A.J. Hart, S. Kumar, Multifunctional performance of carbon nanotubes and graphene nanoplatelets reinforced PEEK composites enabled via FFF additive manufacturing, Composer Part B-Eng 184 (2020) 107625, https://doi.org/10.1016/j.compositesb.2019.107625.

[47] S. Fudger, D. Sediako, P. Karandikar, C.Y. Ni, Residual stress induced mechanical property enhancement in steel encapsulated light metal matrix composites, Mat Sci Eng a-Struct 699 (2017) 10–17, https://doi.org/10.1016/j.msea.2017.05.073.

[48] F. Jasempoor, H. Elmkhah, O. Imantalab, A. Fattah-alhosseini, Improving the mechanical, tribological, and electrochemical behavior of AISI 304 stainless steel by applying CrN single layer and Cr/CrN multilayer coatings, Wear 504 (2022) 204425, https://doi.org/10.1016/j.wear.2022.204425.

[49] Y. Isono, T. Namazu, N. Terayama, Development of AFM tensile test technique for evaluating mechanical properties of sub-micron thick DLC films, J. Microelectromech. Syst. 15 (2006) 169–180, https://doi.org/10.1109/Jmems.2005.859196.

[50] C.A. Griffiths, A. Rees, R.M. Kerton, O.V. Fonseca, Temperature effects on DLC coated micro moulds, Surf. Coating. Technol. 307 (2016) 28–37, https://doi.org/10.1016/j.surfcoat.2016.08.034.

[51] S.Y. Li, H. Li, G.S. Ma, J. Wei, G.X. Zhou, Y. Zhang, P. Guo, P.L. Ke, A.Y. Wang, Dense Cr/GLC multilayer coating by HiPIMS technique in high hydrostatic pressure: microstrusctural evolution and galvanic corrosion failure, Corros. Sci. 225 (2023) 111618, https://doi.org/10.1016/j.corsci.2023.111618.

[52] C.Q. Dang, J.L. Li, Y. Wang, J.M. Chen, Structure, mechanical and tribological properties of self -toughening TiSiN/Ag multilayer coatings on Ti6A14V prepared by arc ion plating, Appl. Surf. Sci. 386 (2016) 224–233, https://doi.org/10.1016/j.apsusc.2016.06.024.

[53] J. Hu, Y.K. Chou, A numerical study of interface behavior of diamond coated cutting tools, Transactions of NAMRI/SME 36 (2008) 533–540.

[54] C. Chen, X. Xie, Y. Xie, X. Yan, C. Huang, S. Deng, Z. Ren, H. Liao, Metallization of polyether ether ketone (PEEK) by copper coating via cold spray, Surf. Coating. Technol. 342 (2018) 209–219, https://doi.org/10.1016/j.surfcoat.2018.02.087.

[55] R. Goltsberg, I. Etsion, Contact area and maximum equivalent stress in elastic spherical contact with thin hard coating, Tribol. Int. 93 (2016) 289–296, https://doi.org/10.1016/j.triboint.2015.09.034.

[56] R. Goltsberg, I. Etsion, A model for the weakening effect of very thin hard coatings, Wear 308 (2013) 10–16, https://doi.org/10.1016/j.wear.2013.09.019.

[57] Y.H. Wang, C.H. Wang, C. You, W.D. Cheng, M.L. Dong, Z.Y. Zhu, J.Q. Liu, L. Wang, X.D. Zhang, Y. Wang, Analysis on thermal stress of optimized functionally graded coatings during thermal shock based on finite element simulation, Mater. Today Commun. 35 (2023) 105699, https://doi.org/10.1016/j.mtcomm.2023.105699.

[58] A. Favache, A. Daniel, A. Teillet, T. Pardoen, Performance indices and selection of thin hard coatings on soft substrates for indentation and scratch resistance, Mater. Des. 176 (2019) 107827, https://doi.org/10.1016/j.matdes.2019.107827.

[59] H. Chai, Fracture mechanics analysis of thin coatings under spherical indentation, Int. J. Fract. 119 (2003) 263–285, https://doi.org/10.1023/A:1023913927118.

[60] S. Novak, M. Kalin, P. Lukas, G. Anne, J. Vleugels, O. Van der Biest, The effect of residual stresses in functionally graded alumina-ZTA composites on their wear and friction behaviour, J. Eur. Ceram. Soc. 27 (2007) 151–156, https://doi.org/10.1016/j.jeurceramsoc.2006.01.021.

[61] D. Neerinck, P. Persoone, M. Sercu, A. Goel, D. Kester, D. Bray, Diamond-like nanocomposite coatings (a-C:H/a-Si:O) for tribological applications, Diam. Relat. Mater. 7 (1998) 468–471, https://doi.org/10.1016/S0925-9635(97)00201-X.

[62] F. Awaja, R. Guarino, M. Tripathi, M. Fedel, G. Speranza, A.B. Dalton, N.M. Pugno, M. Nogler, Tuning the tribological performance of plasma-treated hybrid layers of PEEK-GO-DLC, Tribol. Int. 176 (2022) 107915, https://doi.org/10.1016/j.triboint.2022.107915.

[63] Y.T. Zhao, D.Q. He, W.S. Li, Q. Song, H.M. Zhai, B. Cheng, The role of cermet interlayer on tribological behaviors of DLC/Cr3C2-NiCr duplex coating from the perspective of carbonaceous transfer film formation, Ceram. Int. 48 (2022) 36945–36952, https://doi.org/10.1016/j.ceramint.2022.08.261.

[64] Y.X. Wang, F.Y. Yan, A study on tribological behaviour of transfer films of PTFE/bronze composites, Wear 262 (2007) 876–882, https://doi.org/10.1016/j.wear.2006.08.026.

[65] S.M. Yeo, A.A. Polycarpou, Fretting experiments of advanced polymeric coatings and the effect of transfer films on their tribological behavior, Tribol. Int. 79 (2014) 16–25, https://doi.org/10.1016/j.triboint.2014.05.012.

[66] W.J. Yang, Y.-H. Choa, T. Sekino, K.B. Shim, K. Niihara, K.H. Auh, Thermal stability evaluation of diamond-like nanocomposite coatings, Thin Solid Films 434 (2003) 49–54, https://doi.org/10.1016/s0040-6090(03)00466-8.